J. Fluid Mech. (1998), *vol.* 369, *pp.* 23–48. Printed in the United Kingdom

The influence of rotation on shelf convection

By P. JACOBS AND G. N. IVEY

Centre for Water Research, The University of Western Australia, Nedlands, Perth, Western Australia 6907
e-mail: jacobsp@cwr.uwa.edu.au

(Received 10 October 1997 and in revised form 27 March 1998)

A series of laboratory experiments was conducted to study the flows and exchange processes generated by turbulent convection in a shallow fluid with a combination of a shelf and slope topography in the presence of rotation. For convenience, heat loss at the ocean surface was modelled by heating from below with a buoyancy flux B_0 applied to a circular portion (of radius R) of the base of a cylindrical tank, rotating with angular frequency f. The working volume was closed by an inverted model of a shelf and slope topography (with slope angle ϕ), creating a fluid height H between the forced surface and the shelf. After the initiation of the buoyancy forcing, the average temperature in the actively convecting region initially increases linearly with time but slows down once a lateral heat flux is generated by baroclinic instability at the edge of the convecting region. The wavelength of this instability is described by $\lambda = (5.9 \pm 0.3)$ R_D, with R_D the Rossby radius of deformation, defined by $(g'H)^{1/2}/f$, where g' is the reduced gravity based on the density difference between the convecting and ambient fluids. A steady state is eventually reached when the lateral heat flux balances the (vertical) heat flux due to the forcing. The results differ from previous work in either unbounded or in constant-depth environments. It is shown that the steady-state density anomaly between the convecting and ambient regions is given by $g'_f = (1.6 \pm 0.2)$ $(B_0 f)^{1/2}$ (R/H), while the time to reach this steady state is $\tau = (3.1 \pm 0.5)$ $(f/B_0)^{1/2}$ R. The eddy velocity, characterizing the lateral exchange process, is given by $v_{flux} \approx 1.2$ $(B_0/f)^{1/2}$. These results are consistent with the description of the lateral exchange process by eddy diffusion (rather than advection). Comparisons are made between the experimental results and field observations of convection events.

1. Introduction

Intense cooling of the surface layers of the ocean due to strong, cold winds occurs in high-latitude seas, for example the Labrador Sea in the Arctic (Clarke & Gascard 1983) and the Weddell Sea in the Antarctic (Gascard 1991), as well as in mid-latitude seas, of which observations in the Mediterranean Sea are best documented (Leaman & Schott 1991 and Schott *et al.* 1996). In response to this intense cooling, large-scale convectively driven flows form in the surface layers. Initially, the effects of the surface cooling stay confined to the region underneath the portion of the surface which is being cooled, forming a well-mixed layer of denser water (this can also be achieved by brine rejection if the cooling is so strong that ice is being formed on the surface). However, if the atmospheric conditions that cause the surface cooling persist for long enough (in the order of several days), horizontal exchange processes will be generated to redistribute the colder water. Previously reported observations and modelling efforts have shown that, in either a constant-depth ocean or in an unbounded but stratified environment, this horizontal exchange is dominated by the baroclinic instability of a

rim current which forms around the periphery of the well-mixed region (Gascard & Clarke 1983; Coates, Ivey & Taylor 1995; Ivey, Taylor & Coates 1995; Raasch & Etling 1997; and the recent review by Maxworthy 1997). The horizontal scale of this instability (the 'eddy' size) is of the order of the Rossby radius, given in the homogeneous case by $R_D = (g'H)^{1/2}/f$, where $g' = g\,\Delta\rho/\rho$ and $\Delta\rho$ is the density anomaly between the mixed layer and the ambient, H is the height of the water column and f is the Coriolis parameter. The instability process will eventually result in a geostrophically turbulent flow field, in which dense fluid is transported away from the convecting region by eddies which pinch off from the forced region and travel throughout the entire domain. A steady state can be reached in the production of convectively stirred fluid when the horizontal heat flux associated with the eddy processes balances the heat loss through the surface. The density anomaly in this steady state, which determines the water mass characteristics of the dense outflow, can depend on the strength of the buoyant forcing, as well as on some geometrical parameters and possibly also the strength of the background rotation.

From laboratory models of isolated convection in a constant-depth ocean, Brickman (1995) and Narimousa (1997) both concluded that the steady-state density anomaly between the convecting and ambient regions is independent of the background rotation. However, Brickman (1995) also pointed out that the horizontal scale of the baroclinic eddies, relative to the size of the forcing region, influences the time it takes to reach a temperature equilibration in the convecting region. This, in turn, will determine the final value of the density anomaly in the core of this region, defined as that portion of the convecting region initially unaffected by the eddying motion. Since the size of the eddies, set by the value of the Rossby radius of deformation R_D, is a function of the rotation rate, the latter parameter can thus influence the steady-state density anomaly indirectly. Jones & Marshall (1993) and Chapman & Gawarkiewicz (1997) indeed found such a dependency in constant-depth numerical models of isolated convection. It is therefore not clear why this dependency has not been recovered in the previously mentioned laboratory models.

If the intense cooling occurs over the surface of a relatively shallow coastal sea, then the presence of the adjacent continental slope will modify the strength and possibly also the lateral position of the baroclinic eddies (e.g. Mory, Stern & Griffiths 1987). Gawarkiewicz & Chapman (1995) described two important effects of the bottom slope: first, it introduces a background potential vorticity gradient, which allows isolated eddies to follow isobaths with the shallower water on their right (in the northern hemisphere); second, there is a downslope component of the gravitational acceleration. Variation of the steepness of the slope in the model of Gawarkiewicz & Chapman (1995) led to the conclusion that this latter effect was the dominant one, since for steeper slopes the offshore movement of the eddies was more rapid. This also resulted in smaller values of the steady-state density anomaly. It is clear that the presence (and steepness) of a sloping bottom can thus affect the exchange of heat and subsequently any tracer transport between the convecting fluid and the ambient fluid offshore.

This paper will address the response of an initially unstratified ocean with shelf and slope topography to a constant surface buoyancy forcing. The main goal of this study is to quantify the role of background rotation on the density and velocity distributions characterizing the convective and lateral mixing processes in such a geometry. In §2, the description of the dynamics of this process leads to some predictions regarding the average temperature in the convecting region, as well as scalings for velocity fields and instability patterns. The predictions arising from these arguments have been tested in a series of laboratory experiments, the setup of which is described in §3. The results of

this physical model are discussed in §4, while in §5 comparisons are made with some field data, and the summary and conclusions are in §6.

2. Dynamical considerations

Consider the situation where we apply a buoyancy forcing B_0 per unit area (in $m^2\ s^{-3}$) over a circular region with radius R (m) and total depth H (m). The buoyancy flux can be related to a heat flux F through $B_0 = g\alpha F/\rho C_P$, with α the thermal expansion coefficient and C_P the specific heat at constant pressure. As previous studies have shown, the Rossby number Ro defined as

$$Ro = \left(\frac{B_0}{f^3 H^2}\right)^{1/3} \tag{1}$$

is a convenient dimensionless group to characterize the convective processes (see e.g. Coates *et al*. 1995). Ro can be interpreted as the ratio of the characteristic time scale for rotationally controlled turbulence (i.e. $1/f$) and the time scale for convection over a depth H in the absence of rotation (i.e. $H/(B_0 H)^{1/3}$). Equally it can be interpreted as the square of the ratio of density differences between the convective mixed fluid and the surrounding waters in the non-rotating and rotating cases, given by

$$g'_{non\text{-}rot} \sim (B_0^2/H)^{1/3} \quad \text{and} \quad g'_{rot} \sim (B_0 f)^{1/2},$$

respectively (Fernando, Chen & Boyer 1991).

Maxworthy & Narimousa (1994) introduced a natural Rossby number with a slightly different form from that in equation (1): $Ro^* = (B_0/f^3 H^2)^{1/2}$ (equal to $Ro^{3/2}$). From observations of large-scale flow features they found that beneath a transition depth, given by $Z_C \approx (12.7 \pm 1.5)\ (B_0/f^3)^{1/2}$, rotation dominates the convective turbulence, resulting in the formation of vertical vortices underneath the source of buoyancy. Non-dimensionalizing this depth by the fluid depth H gives a critical value of $Ro^{*1/2}_{crit} = 0.28$. However, in a recent paper Coates & Ivey (1997), using direct measurements of the small-scale turbulent velocity and temperature fields rather than observations of large-scale flow features, found $Z_C \approx (35 \pm 15)\,(B_0/f^3)^{1/2}$, from which it follows that transition from rotationally *affected* to rotationally *controlled* turbulence occurs in the range $0.14 \leqslant Ro^{*1/2}_{crit} \leqslant 0.22$.

The processes following the onset of the convective forcing can conveniently be separated into three different stages: initially, pure convective overturning; secondly, the onset of lateral exchange; and finally, the steady state, characterized by the fact that the density contrast between the convecting and ambient fluids is no longer changing with time. In the following section, these three stages will be described. The distinctions between these different stages can be defined by considering the buoyancy flux B_{SW} through the cylindrical surface bounding the actively stirred convecting region: in the convective overturning stage $B_{SW} = 0$, the second stage is defined by $0 < |B_{SW}| < |B_0|$, while the final steady state is reached when $|B_{SW}| = |B_0|$.

2.1. *Convective overturning*

For some time immediately after the start of the buoyancy forcing, there is no exchange between the volume directly below the cooled surface (the convecting or forced region) and the exterior ambient fluid, so that the average temperature T in this volume ($V = \pi R^2 H$) decreases due to the extraction of heat at the surface over area $A\,(= \pi R^2)$ according to

$$FA\,\Delta t = Q = \rho C_p\, V \Delta T, \tag{2}$$

with Q the total heat extracted from the fluid in time Δt. For constant forcing B_0 the average temperature in the mixed layer decreases linearly with time, independent of either rotation rate f or size of forcing region R, according to

$$g' = g\alpha\,\Delta T = \frac{B_0\,t}{H}, \tag{3}$$

where we have used the definition of B_0 stated above equation (1). Note that this also describes the temperature decrease of the fluid if the volume below the cooled surface is bounded by insulating sidewalls, as for example in the experiments of Coates & Ivey (1997) (although the time dependency of the temperature measurements is not discussed in this paper) and some initial experiments of Brickman (1995, see his figure 6).

The time scale characterizing this convective overturning stage is given by the time it takes for a fluid parcel with a typical convective (vertical) velocity $(B_0\,H)^{1/3}$ to be displaced over the vertical length scale H:

$$t_{co} \sim H/(B_0\,H)^{1/3} = \left(\frac{H^2}{B_0}\right)^{1/3} \tag{4}$$

and is therefore independent of f.

2.2. *Onset of lateral exchange*

Owing to the increasing lateral temperature (density) difference and hence the increasing available potential energy, the flow field will become baroclinically unstable and some lateral exchange occurs between the convected and ambient regions. Previous studies (Legg & Marshall 1993; Ivey *et al.* 1995; Coates *et al.* 1995; Raasch & Etling 1997) have shown that this exchange is governed by the onset of baroclinic instabilities around the edge of the convected region. In the shelf and slope geometry and when the horizontal extent of the forcing region is at least as large as the width of the shelf, the initial lateral exchange will be formed by an outflow of dense water onto the sloping bottom. Mory *et al.* (1987), Whitehead *et al.* (1990) and Hill (1996), among others, have described how this outflow induces a strong cyclonic motion in the initially quiescent upper layer of ambient fluid. Furthermore, the background potential vorticity gradient due to the presence of the slope will influence any cross-slope movement of fluid columns, possibly resulting in an along-slope flow (see also Lane-Serff & Baines 1998). This mechanism constitutes a major difference from constant-depth models, in which there is no inhibition of the tendency for the baroclinic eddies to move away from the convected region, for example.

In this phase of development, some heat is exchanged between the convecting and ambient regions due to the presence of the developing baroclinic eddies. Since not all the surface heat loss is compensated, the average temperature of the fluid in the convecting region continues to decrease, as in the first stage, although this now occurs at a reduced rate than given by (3).

The baroclinic eddies are characterized by a length scale of the order of the Rossby radius of deformation, given by

$$R_D = \frac{(g'\,H)^{1/2}}{f}. \tag{5}$$

Note that since g' is still increasing with time, so is the typical eddy size. The efficiency with which the entire convected region can be 'swept clean' by the baroclinic processes

depends on the size of the eddies relative to the size of the cooled surface R during this intermediate stage. When R_D is relatively large (e.g. for low rotation rate), a large portion of the convecting region is directly affected by the eddy transports and it can therefore be expected that the average temperature in the forced region will not decrease much further before a steady state is reached. However, for small values of R_D/R (for example in the case of strong background rotation), only a narrow band of width R_D around the edge of the forced region is directly affected by the eddy motions at this stage. The inner portion of the fluid below the cooled surface is effectively screened off from the ambient fluid by the ring of baroclinic eddies, generated at the periphery, and the temperature of this core fluid can continue to decrease for some time. These processes will continue until a balance is reached between the energy loss through the surface and the lateral heat flux into the convected region effected by the baroclinic eddies. The final value of the temperature difference between the forced (mixed) region and the quiescent ambient region, reached at the start of the steady state, must therefore depend on the strength of the background rotation, as for example found by Jones & Marshall (1993) and Send & Marshall (1995), but contrary to the results of for example Brickman (1995), Legg, Jones & Visbeck (1996) and Visbeck, Marshall & Jones (1996).

Here we will simply state that any f-dependency of the final density difference (the density difference reached at the end of this transient state) for a fixed slope angle ϕ is a result of the governing dynamics during the transient state of the convection process. Then suppose that at the end of this transient state the final density anomaly can be described by

$$g'_f \sim B_0^{\alpha} f^{\beta} R^{\gamma} H^{\delta} \tag{6}$$

with the restrictions (from dimensional analysis)

$$3\alpha + \beta = 2, \tag{7}$$

$$2\alpha + \gamma + \delta = 1. \tag{8}$$

A time scale τ can then be defined as the point on the time axis of a g' vs. t graph at which the linear increase with time (during the convective overturning state) crosses the horizontal line of the value of g'_f (see also Brickman 1995). It follows from equations (3) and (6) that

$$\tau \sim B_0^{\alpha-1} f^{\beta} R^{\gamma} H^{\delta+1} \tag{9}$$

which gives an indication of the time at which steady state is reached.

2.3. *Steady state*

At steady state, the energy loss through the surface will be completely compensated by the heat flux through the sidewalls of the convecting region (the chimney). The energy balance is then expressed by (see e.g. Visbeck *et al.* 1996)

$$B_0 \pi R^2 = n \int_0^H \int_0^{\lambda} \overline{v'g'}\, \mathrm{d}s\, \mathrm{d}z \sim n\lambda H \overline{v'g'} = 2\pi R H \overline{v'g'}, \tag{10}$$

where n is the number of eddies around the circumference of the chimney, λ is the wavelength of the baroclinic eddies ($= 2\pi R/n$), $\overline{v'g'}$ is the lateral eddy-driven buoyancy flux, s is the path length around the circumference and z is the vertical coordinate. From (10) we see that

$$\overline{v'g'} \sim \frac{B_0 R}{H}. \tag{11}$$

Visbeck *et al.* (1996) and Whitehead, Marshall & Hufford (1996) assumed that the velocity scale in (11) is of the order of the internal wave speed, i.e. $\overline{v'g'} \sim (g'H)^{1/2}g'$ or, in the stratified case, $\overline{v'g'} \sim NhN^2h = N^3h^2$, where N is the buoyancy frequency of the (undisturbed) background stratification and h the instantaneous depth of the convecting layer. Coates *et al.* (1995) have shown that the characteristic mean velocity of the rim current is equal to this wave speed. However, it is not obvious why the eddy velocity characterizing the exchange process normal to the direction of this mean flow in the rim current should be of the same order of magnitude as the mean flow itself, even in a flat bottom geometry. Furthermore, in the case of a shelf and slope topography, the characteristic velocity for the lateral exchange could be influenced by the strength of the cyclonic circulation generated in the upper layer by the dense outflow onto the slope (Mory *et al.* 1987 and Lane-Serff & Baines 1998). In general, we can parameterize the lateral buoyancy flux at steady state by the product of the velocity scale of the radial flux across the frontal position $r = R$ and the bulk density difference between the convecting and ambient fluids in steady state

$$\overline{v'g'} \sim v_{flux}g'_f. \tag{12}$$

Then, using (6), (11) and (12), v_{flux} can be described as

$$v_{flux} \sim B_0^{1-\alpha}f^{-\beta}R^{1-\gamma}H^{-1-\delta}. \tag{13}$$

We now set out to describe the experimental setup and results, carried out to quantify some of the above predictions, in particular (6), (9) and (13).

3. Physical model

3.1. *Setup and experimental parameters*

The experiments were performed in a cylindrical tank with radius $R_{tank} = 0.48$ m, mounted on a rotating table (figure 1). For experimental convenience, the fluid was heated from below rather than cooled from above. The tank was fitted with a false bottom with built-in circular copper plate of radius $R = 0.20$ m that acted as a heat exchanger. The plate could be heated by pumping relatively hot fluid from a constant-temperature bath through a circuit of pipes built into the copper plate. The plate was insulated on the sides and the bottom, so that heat could only escape through the top surface. The heat flux F (and therefore the buoyancy flux B_0) was measured from the temperature drop and volume flow rate of the fluid passing through the heated plate. Thermistors were placed at the inlet and outlet ports of the heat exchanger to determine the temperature drop, while a rotor-type flowmeter was used to monitor the (constant) volume flow rate. With this system, the heat flux could be determined with an accuracy of about 6%. Errors in the values of the buoyancy flux are somewhat larger (up to 10%), mainly because of the sensitivity of the thermal expansion coefficient to temperature changes.

The working section of the tank was closed with a model of a shelf and slope (slope angle $\phi = 28°$). The radius of the shelf region was equal to the radius of the heat exchanger, so that the shelf break coincided with the edge of the heat exchanger. The vertical position of the lid could be varied in order to change the height H of the fluid column below the shelf. Finally, the cylindrical tank was surrounded by a slightly larger octagonal one (not shown in figure 1), with the volume between the two tank walls filled with water at the same temperature as the water in the working section (approximately room temperature) to minimize optical distortion through the curved wall of the working tank.

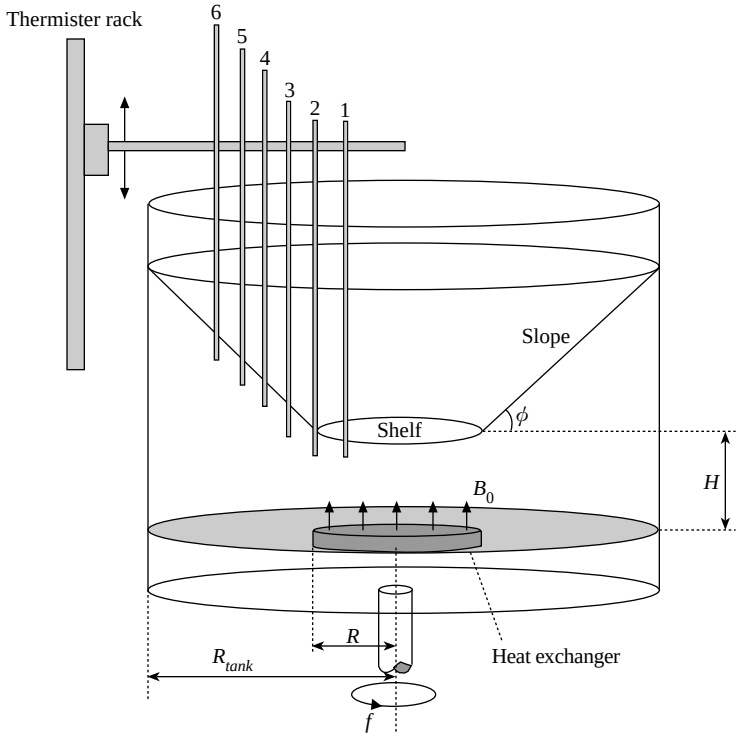

FIGURE 1. Sketch of experimental setup.

Experimental number	B_0 ($m^2\ s^{-3}$)	f (s^{-1})	H (m)	Ro (−)	Ro_R (−)	ΔT_{final} (°C)	R_D (m)	Mode number
5	1.60×10^{-6}	0.424	0.08	0.149	0.151	1.4 ± 0.3	0.039	5
6	1.65×10^{-6}	0.212	0.08	0.300	0.257	1.0 ± 0.2	0.066	3
7	1.53×10^{-6}	0.322	0.08	0.193	0.184	1.51 ± 0.26	0.051	5
8	1.67×10^{-6}	0.100	0.08	0.639	0.452	0.65 ± 0.24	0.111	2
9	1.21×10^{-6}	0.504	0.08	0.113	0.124	1.29 ± 0.24	0.032	7
10	1.59×10^{-6}	0.100	0.04	0.999	0.447	1.04 ± 0.27	0.099	2
11	1.61×10^{-6}	0.300	0.04	0.334	0.196	2.29 ± 0.43	0.050	5
12	1.45×10^{-6}	0.500	0.04	0.193	0.130	2.93 ± 0.40	0.034	6
14	1.57×10^{-6}	0.402	0.04	0.247	0.157	2.56 ± 0.47	0.039	6
15	1.60×10^{-6}	0.640	0.04	0.157	0.111	3.43 ± 0.57	0.027	7
16	1.87×10^{-6}	0.210	0.04	0.501	0.267	1.84 ± 0.37	0.064	3
17	9.29×10^{-7}	0.900	0.04	0.092	0.075	2.85 ± 0.50	0.018	10
18	1.64×10^{-6}	1.204	0.04	0.083	0.070	4.68 ± 0.80	0.017	11
19	1.17×10^{-6}	0.424	0.08	0.134	0.140	2.13 ± 0.31	0.041	5
20	1.21×10^{-6}	0.634	0.08	0.091	0.104	2.55 ± 0.31	0.030	8
21	1.16×10^{-6}	0.900	0.08	0.063	0.079	3.19 ± 0.25	0.024	9
22	1.15×10^{-6}	0.158	0.08	0.357	0.292	1.16 ± 0.18	0.083	3

TABLE 1. Overview of experimental parameters. The radius of the forcing region $R = 0.20$ m and the slope angle $\phi = 28°$ is the same for all experiments

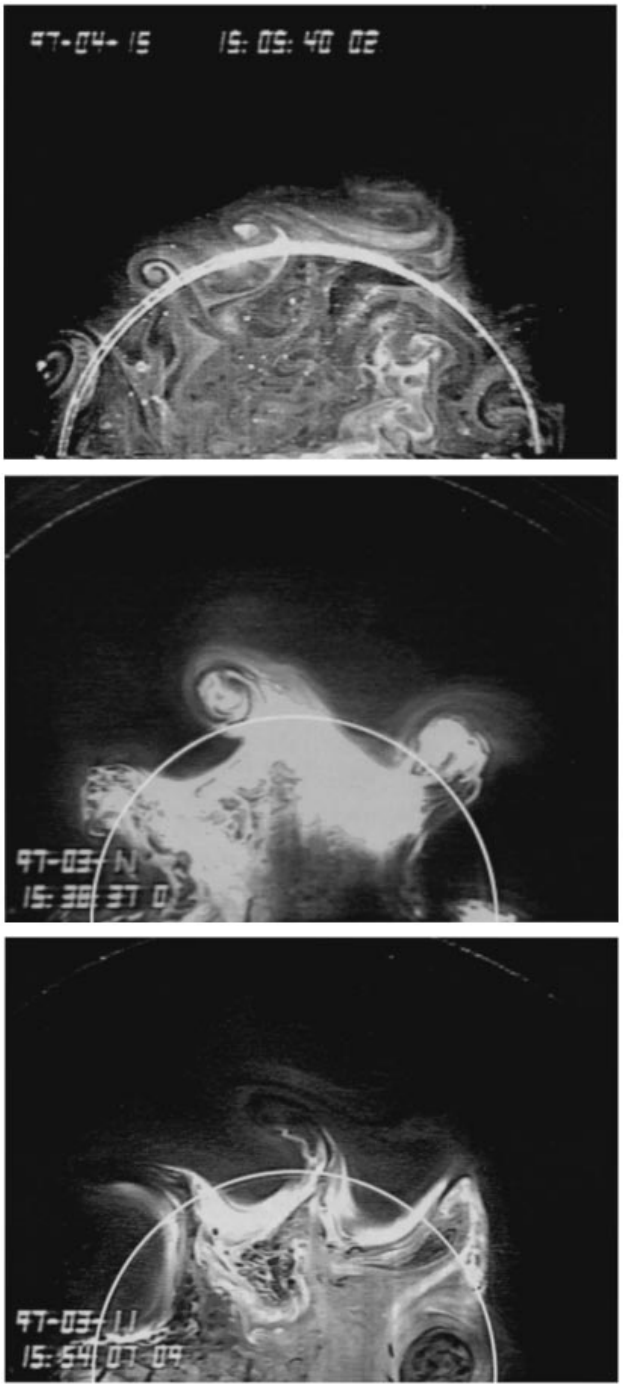

FIGURE 2. Three examples of eddy patterns generated at the edge of the convecting region. Approximately half of the working tank is shown. The edge of the convecting region is indicated by the white semicircle. (*a*) Experiment 18 at $t = 1859$ s ($= 178T$) and $z = 0.02$ m, with typically 11 eddies around the circumference. (*b*) Experiment 12 at $t = 215$ s ($= 8.6T$) and $z = 0.02$ m, with six large eddies around the circumference. (*c*) The same experiment as in (*b*), but now at $t = 1145$ s ($= 43.2T$) and at $z = 0.01$ m. Experiment parameters are listed in table 1.

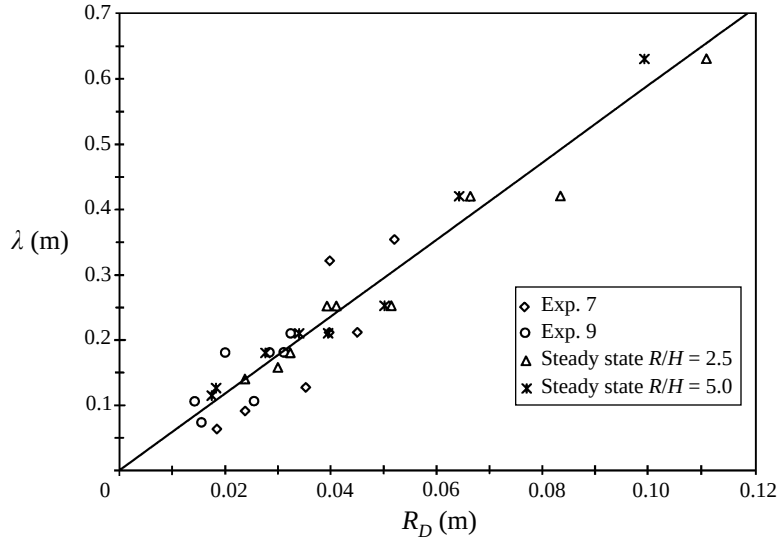

FIGURE 3. Wavelength of baroclinic instabilities as function of the Rossby radius of deformation: temporal values for two experiments and steady-state values for all experiments. The solid line is a best fit, indicating $\lambda = (5.9 \pm 0.3)\ R_D$ (correlation coefficient = 0.921).

Before the start of an experiment, the working fluid was brought to solid-body rotation (rotation rate f). At time $t = 0$, the experiment was initiated by pumping warm water of a constant input temperature through the heat exchanger, thus supplying a buoyancy flux B_0 to the working fluid. The flux B_0 was measured and essentially constant after an initial adjustment period of about 50 s. Measurements showed that after the adjustment period the buoyancy flux decreased slowly due to the decreasing temperature difference between the heated plate and the convecting fluid. This exponential decrease resulted in a typical drop of 10% in the period 100–500 s and a further 4% in the period 500–1000 s. The values in table 1 are the average values for the period 100–1000 s. As discussed above, the problem is determined by a set of five initial parameters (B_0, f, R, H and ϕ), as indicated in figure 1. In the present set of experiments, f and H have been systematically varied (see table 1) to obtain a large range of values for the Rossby number Ro.

3.2. *Measurement techniques*

A set of six thermistors was used to monitor the temperature at fixed radial locations $R_{therm} = [0.15, 0.20, 0.25, 0.30, 0.35, 0.40]$ m for experiments 5–18. For experiments 19–22 the thermistor positions were $R_{therm} = [0, 0.05, 0.10, 0.15, 0.20, 0.40]$ m to obtain a higher spatial sampling density in the actively convecting region. The thermistors could either be used in continuous mode at a sampling frequency of 2 Hz or in a profiling mode at traversing speed 10 cm s^{-1} and sampling at 100 Hz. When operating in continuous mode, each thermistor was positioned at 1.0 cm below the lid at that particular radius for experiments 5–18 (see figure 1). For experiments 19–22, all thermistors were located 5 cm above the bottom of the tank.

To obtain quantitative information on velocity fields, the fluid was seeded with neutrally buoyant particles for experiments 14 and following. Illumination of the fluid in either a horizontal or vertical plane was achieved by the use of a thin sheet of laser

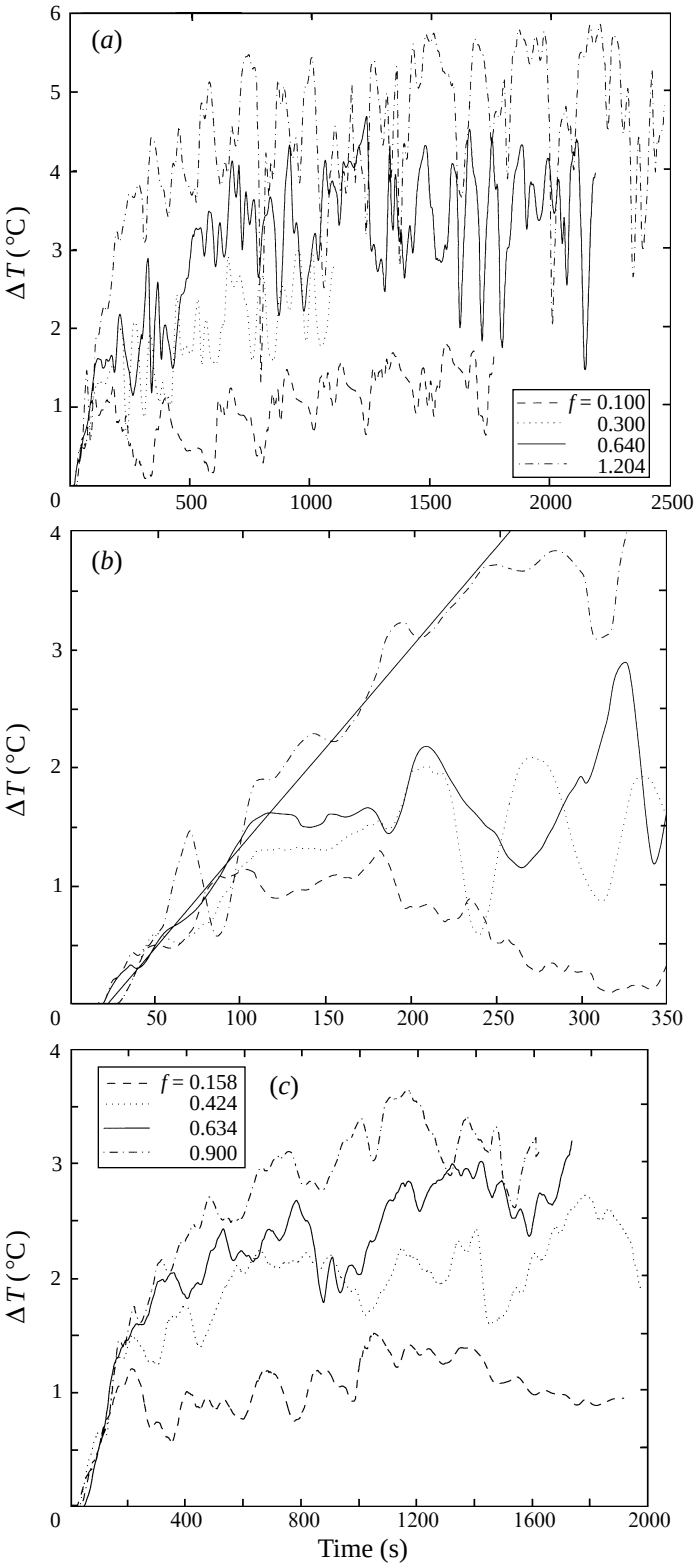

FIGURE 4. For caption see facing page.

light. The height of the horizontal sheet could be varied continuously during the experiment, while the vertical light sheet always passed through the centre of the tank. The motion of the fluorescing particles was recorded by a CCD video camera and stored on a S-VHS video tape. Detailed velocity measurements could then be made using the PIV technique implemented by Stevens & Coates (1994) and described in more detail by Coates & Ivey (1997). Further qualitative information on the flow patterns was obtained by injecting fluorescent dye in the convecting region, either prior to or during the experiment.

4. Results

4.1. *Observations of the developing flow field*

Following the onset of the buoyancy forcing, a mixing layer starts to grow above the heated plate and fills the volume above the forcing area on a time scale given by (4). The range of Rossby numbers Ro corresponded to values for $Ro^{*1/2}$, as defined by Maxworthy & Narimousa (1994), between 0.13 and 1.00 (see also table 1). However, no vertical vortices were observed to form above the mixing layer, indicating that for $Ro^{*1/2} \approx 0.15$ the convection is still not controlled by rotation. This is consistent with the higher value of the constant for the critical depth relation (see §2) as found by Coates & Ivey (1997). So all our experiments were performed in the regime where rotation does not control the turbulent convection itself. Initial lateral exchange processes are then generated, marked by a radial outflow at the top of the mixed layer (at the shelf break) and a radial inflow at the base (see Raasch & Etling 1997 for a detailed description of these radial fluxes in a stratified fluid). The radial outflow of buoyant fluid over the slope develops into an anticyclonic rim current due to the background rotation, as in the experiments of Coates *et al.* (1995) and Ivey *et al.* (1995). The rim current quickly becomes unstable to baroclinic instabilities, resulting in the formation of a regular pattern of more or less isolated lenses of buoyant fluid over the slope. This, in turn, generates strong cyclonic motions in the initially quiescent ambient fluid (Mory *et al.* 1987; Whitehead *et al.* 1990). Contrary to the numerical results of Gawarkiewicz & Chapman (1995), the buoyant lens/cyclone pairs do not move down the slope, but exhibit along-slope motion (with the shallow water to their right) and the whole pattern precesses anticyclonically around the edge of the heated plate for the duration of the experiment. Some examples of the cyclonic baroclinic eddies containing convected fluid are shown in figure 2. These examples show clearly that (i) the eddy size depends on the Coriolis parameter (compare figures 2*a* and 2*b*); (ii) the eddies do not detach from the shelf break and upper slope region; and (iii) the eddies are coherent over very long times (compare figures 2*b* and 2*c*, taken from the same experiment at respectively 8.6 and 43.2 rotation periods after the start of the buoyancy forcing).

The wavelength of the baroclinic eddies is a function of the Rossby radius (cf. Coates & Ivey 1998), which in itself evolves in time as it is determined by the value of the lateral temperature difference and hence the density anomaly between the developing mixing layer and the ambient. In figure 3, the instantaneous wavelengths measured

FIGURE 4. (*a*) Continuous time series of temperature rise above the heated plate for experiments with Coriolis parameter f (in s^{-1}) as indicated: ----, exp. 10; · · · · · ·, exp. 11; ——, exp. 15; -·-·-, exp. 18. (*b*) Close up of the first 350 s for the same experiments as in (*a*). The straight line, with an inclination of $B_0/g\alpha H$, is included for comparison. (*c*) Temperature time series for experiments 22 (----), 19 (· · · · ·), 20 (——) and 21 (-·-·-) with modified radial positions of the thermistors, as described in §3. All data are 30 s running averages of the original thermistor readings to filter the highest frequencies.

during two experiments are plotted against the instantaneous values of the Rossby radius, as well as the steady-state values of all experiments. The correlation is apparent and the least-squares fit results in

$$\lambda = (5.9 \pm 0.3)\, R_D \tag{14}$$

which agrees well with the result of Brickman (1995), who found a constant of 5.7 ± 0.9. The numerical experiments of Gawarkiewicz & Chapman (1995) indicate a constant of proportionality of approximately 5, similar to the one found by Jones & Marshall (see figure 10 in Coates & Ivey 1998). An experimental study investigating the collapse of a chimney of dense fluid and the subsequent break-up into baroclinic eddies presented by Saunders (1973) indicated a constant of 4.3 ± 0.8. So all these results confirm a constant of proportionality of order 5. However, as one reviewer pointed out, related experiments by Mason (1975) and Bastin & Read (1997) indicated that the size of baroclinic eddies over a slope might increase compared with eddies in the constant-depth case. The slightly higher value for the present experiments might be an indication of this effect. All the above mentioned studies were run with initially homogeneous fluid. In contrast, a number of studies with initially linear density stratification have been conducted, where the definition of R_D is now given by $R_D = Nh_{max}/f$, with N the buoyancy frequency of the initial (linear) stratification and h_{max} the steady-state value of the depth of the convecting layer. Coates *et al.* (1995) found a value for the constant of proportionality of 1.5 ± 0.5, Whitehead *et al.* (1996) give the constant as 2.3, Coates & Ivey (1998) found 1.6 and the numerical model of Raasch & Etling (1997) indicated a value of 1.52. While dynamically similar processes occur, there are thus differences in the constant of proportionality relating λ and R_D for the unstratified and stratified cases.

4.2. *Temperature measurements*

The three stages in the response of the convecting fluid, as described in §2, can be identified in figure 4(*a*, *b*), where the temperature rise over the heated plate is shown for four different values of the Coriolis parameter (experiments 10, 11, 15 and 18). Figure 4(*b*) shows in detail the first 350 s of the data plotted in figure 4(*a*). The data are all from thermistor measurements inside the convecting region (at 5 cm from the edge of the heated plate) and are smoothed with a running average over 30 s to eliminate the highest frequencies. In addition, we show in figure 4(*c*) temperature data from experiments 19–22 in which more thermistors were located in the convecting region (see also figure 5*c* further below). The data in figure 4(*c*) are the averaged readings of the thermistors at radial locations 0, 5 and 10 cm from the tank centre.

Three features are clearly seen in figure 4. First, and particularly clear in figure 4(*b*), is the initial linear increase of temperature with time during the state of convective overturning (the solid line with slope $B_0/g\alpha H$, see equation (3), is included for comparison). Secondly, the time at which the temperature signal starts to deviate from the linear increase clearly depends on the rotation rate. Finally, figures 4(*a*) and 4(*c*) show that the final value of the steady-state temperature difference is f-dependent and in fact increases with increasing f. This qualitative observation confirms earlier work on shelf convection by Sugimoto & Whitehead (1983) and Whitehead (1993), but is different from the constant-depth models of for example Brickman (1995), Visbeck *et al.* (1996) and recent work by Narimousa (1997) who all concluded that the steady-state density anomaly is f-independent. The quantitative aspects of this important result will be discussed further below.

Figure 5 shows examples of time series of the individual thermistor data for three experiments with different rotation rates (figure 5*a*: exp. 10, $f = 0.100\ \mathrm{s}^{-1}$, figure 5*b*:

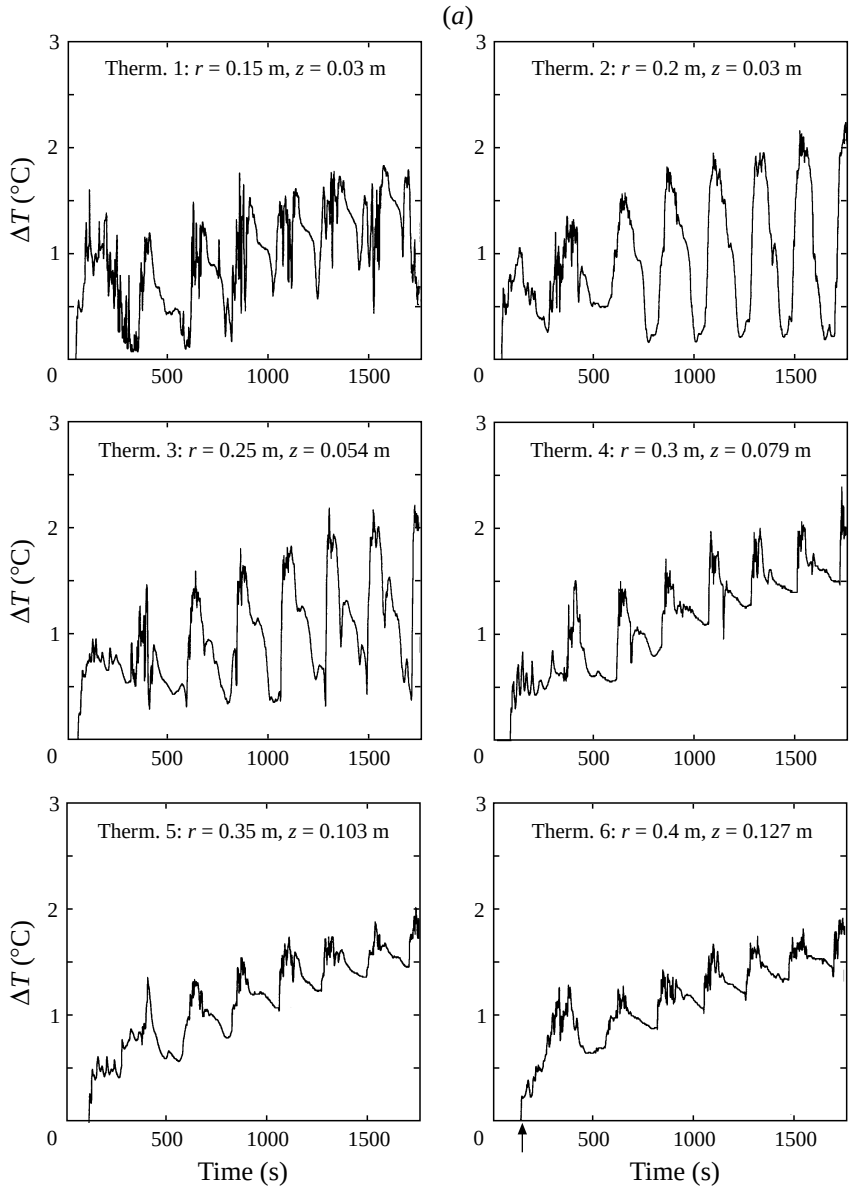

FIGURE 5(*a*). For caption see p. 37.

exp. 12, $f = 0.500\ \mathrm{s}^{-1}$ and figure 5*c*: exp. 21, $f = 0.900\ \mathrm{s}^{-1}$). Recall that for experiments 10 and 12 only thermistor 1 (upper left panels in figures 5*a* and 5*b*) is located inside the convecting region. The wavelike variability in the signals is caused by the background precession motion of the eddy pattern. At one moment, the radial line along which the thermistors are positioned intersects a part of an eddy where the flow is directed out of the convecting region and so the measured temperature is relatively high. Some time later, the thermistor line intersects the other side of the eddy, where the flow is radially inward and relatively cold ambient fluid is drawn into the convecting region. Figure 5(*b*) shows a higher variability than figure 5(*a*), which is caused by the different number of eddies around the circumference of the forced region

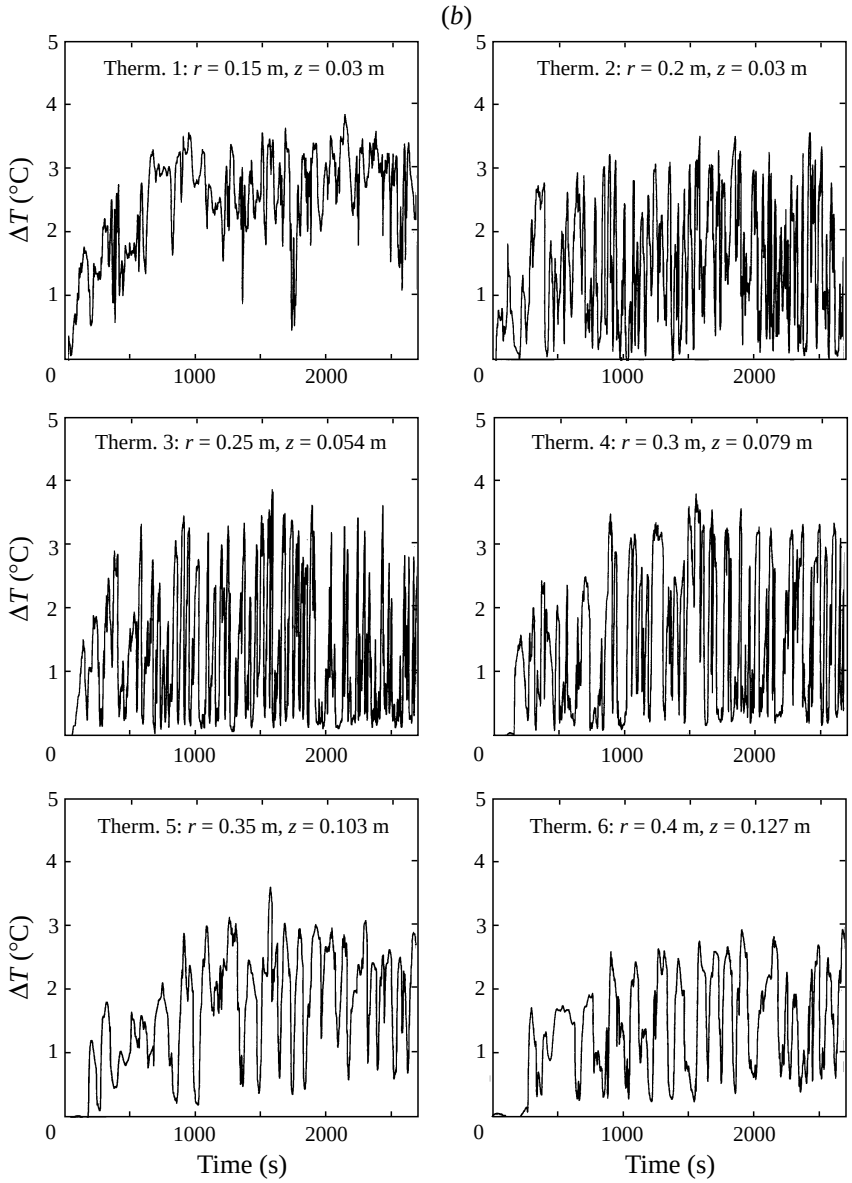

FIGURE 5(*b*). For caption see p. 37.

(see table 1). Figure 5(*c*) is included to show that (i) well inside the convecting region, the temperature measurements are independent of the radial position (thermistors 1–4), and (ii) the temperature of the ambient fluid does not increase significantly during the experiment (thermistor 6).

In figure 6 we plot the arrival time of convected fluid at each of the thermistors for the experiments with $R/H = 5$. It is defined as the time of the first temperature increase registered at each thermistor since the start of the forcing. The arrival time increases considerably for higher background rotation, indicating that the rotation restricts the initial outflow onto the slope. This figure also confirms that the strength of the background rotation does not influence the growth of the mixed layer above the heated

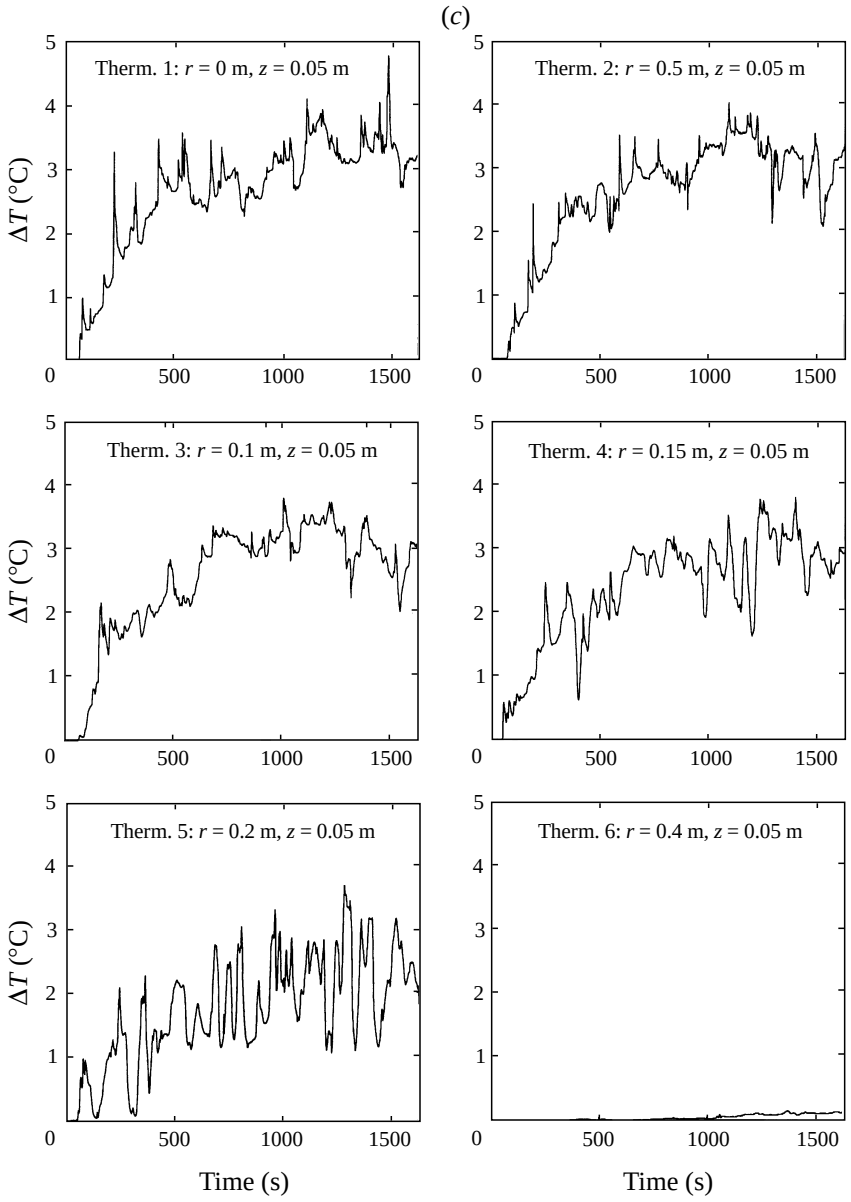

FIGURE 5. Three examples of the continuous temperature output of the thermistors at radial and vertical positions as indicated: (*a*) exp. 10, $f = 0.100\ \mathrm{s}^{-1}$, (*b*) exp. 12, $f = 0.500\ \mathrm{s}^{-1}$ and (*c*) exp. 21, $f = 0.9\ \mathrm{s}^{-1}$. Thermistor positions are indicated above each of the panels. The arrow in the sixth panel of (*a*) indicates the arrival of convected fluid at that particular thermistor location.

plate in the early stages of the experiments (the convective overturning regime) since the arrival times of the thermistors at $r = 0.15$ and 0.2 m are constant over the range of the experiments. This is confirmed by the arrival times for experiments 19–22, where five of the six thermistors were positioned inside the convecting region (see figure 5*c*).

From the measurements of the temperature over the heated plate, we can estimate the steady-state value of the temperature (density) difference between the convecting and ambient regions. For each thermistor the temperature difference is defined as the

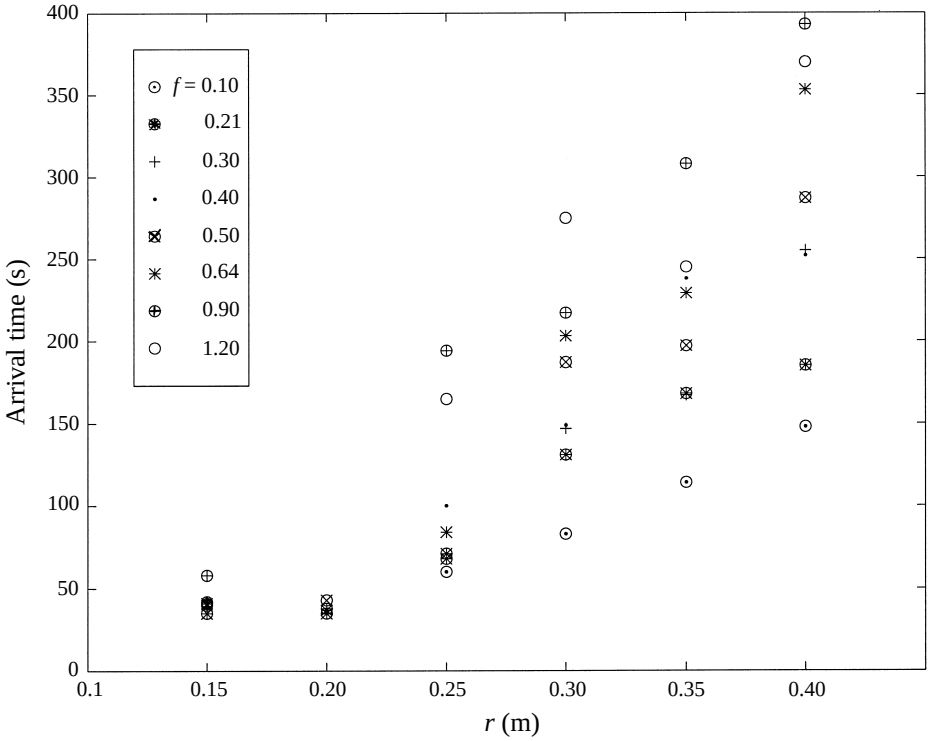

FIGURE 6. Arrival times for convected fluid as function of the radial position of each thermistor for the Coriolis parameter (in s^{-1}) as indicated. Only experiments with $R/H = 5.0$ are included.

temperature rise from the initial value since at $t = 0$ the temperature is uniform throughout the tank and the change in temperature of the ambient fluid is negligible for the duration of the experiment, which is confirmed by panel 6 (bottom right) of figure 5(*c*). The steady-state temperature difference was determined by taking the average of the temperature signals (such as depicted in figures 4*a* and 4*c*) after the flow had reached steady state. The start of this period was estimated by eye. For a few experiments a more quantitative check was made by calculating an average temperature difference over various portions of the steady-state period. Providing the averaging period was long compared with the variability in the temperature signal due to the baroclinic eddies, these independent estimates yielded the same results. The values listed in table 1 are therefore the averages over the entire steady-state period.

Figures 4–6 already give an indication that the steady-state density anomaly will depend on the strength of the background rotation. These and other experimental results are shown in figure 7(*a–c*) in which g'_f is plotted against f. Each subplot comprises a set of experiments in which typical values of B_0 were 4×10^{-8} m^2 s^{-3} in figure 7(*a*), 3×10^{-7} m^2 s^{-3} in 7(*b*) and 1.5×10^{-6} m^2 s^{-3} for the experiments of figure 7(*c*). In each plot a line with slope $+0.5$ is included for comparison. The data, which cover experiments where B_0 varies over two decades, clearly show that $g'_f \sim f^{1/2}$, at least for large enough values of f (see below).

In the present experiments the range of R/H values is too limited to make any definitive conclusions about the dependence of g'_f on R/H. Inclusion of the data of Sugimoto & Whitehead (1983), Whitehead (1993) and the numerical model results of Chapman & Gawarkiewicz (1997), however, extends the range of R/H values over two

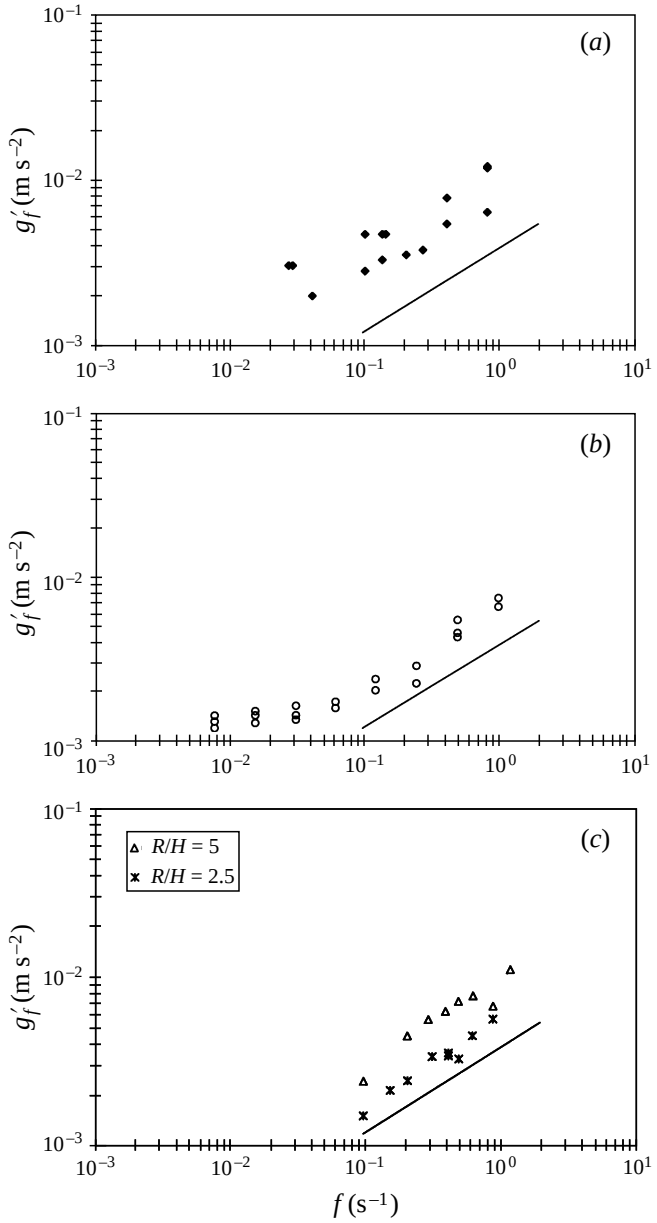

FIGURE 7. Steady-state values of the density anomaly between the convected region and the ambient as a function of Coriolis parameter for three experimental series: (*a*) data from Sugimoto & Whitehead (1983), with $2.0\times10^{-8} < B_0 < 6.4\times10^{-8}$ m^2 s^{-3} and $R/H = 18$; (*b*) data from Whitehead (1993), with $B_0 = 2.7\times10^{-7}$ m^2 s^{-3} and $R/H = 2.8$ and (*c*) present data, with $0.9\times10^{-6} < B_0 < 1.9\times10^{-6}$ m^2 s^{-3} and values of the aspect ratio R/H as indicated. The solid line in each of the subplots has a slope of $+0.5$.

decades. Figure 8 shows that the best fit line through this extended set of data has a slope $n = 1.01\pm0.04$. In summary, the present results suggest a best fit of the form

$$g'_f = (1.6\pm0.2)(B_0 f)^{1/2}(R/H)^1. \tag{15}$$

It then follows from (6)–(9) that the steady-state time scale can be described by

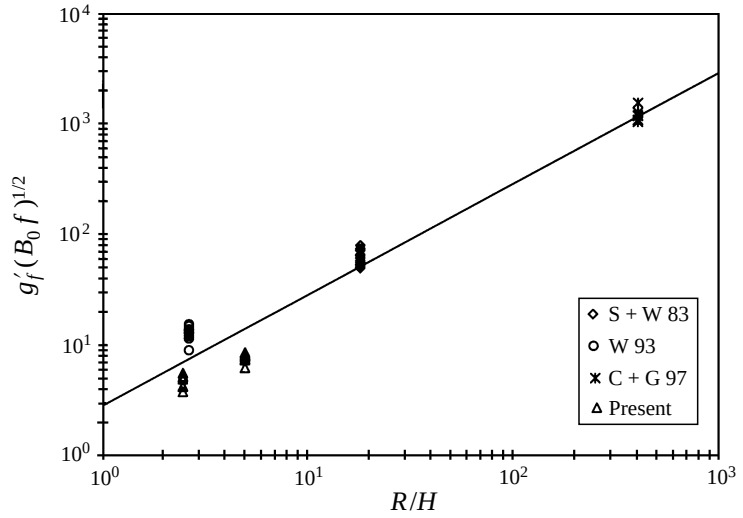

FIGURE 8. Steady state-density anomaly, non-dimensionalized by $(B_0 f)^{1/2}$, as function of the aspect ratio R/H from the present experiments and from Sugimoto & Whitehead (1983; S+W 83), Whitehead (1993; W 93) and Chapman & Gawarkiewicz (1997; C+G 97). The best fit line has a slope 1.01 ± 0.04, with correlation coefficient 0.936.

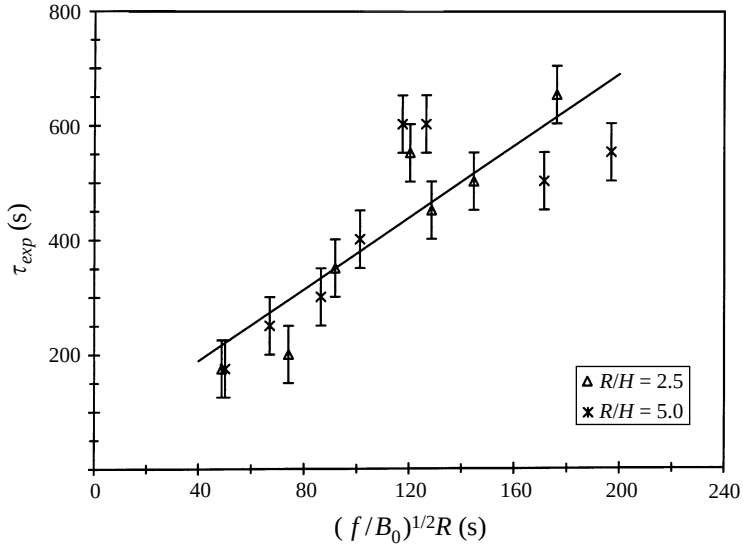

FIGURE 9. Variation of the time to reach steady state (estimated from experimental data such as shown in figure 4*a*, *c*) with the prediction from equation (16), $\tau \sim R(f/B_0)^{1/2}$. The linear regression indicated by the solid line suggest a constant of proportionality of 3.1 ± 0.5 (correlation coefficient 0.728).

$\tau \sim (f/B_0)^{1/2} R$. In figure 9 we plot the experimental steady-state time, estimated from figures such as 4(*a*, *c*), against this prediction. The best fit line suggest a constant of proportionality of 3.1 ± 0.5, so that we find

$$\tau = (3.1 \pm 0.5)\ (f/B_0)^{1/2}\, R. \tag{16}$$

Finally, we note from figure 7(*b*) that the data for $f < 0.1\ \mathrm{s}^{-1}$ show little sensitivity to changes in the Coriolis parameter f. These results can be interpreted as follows:

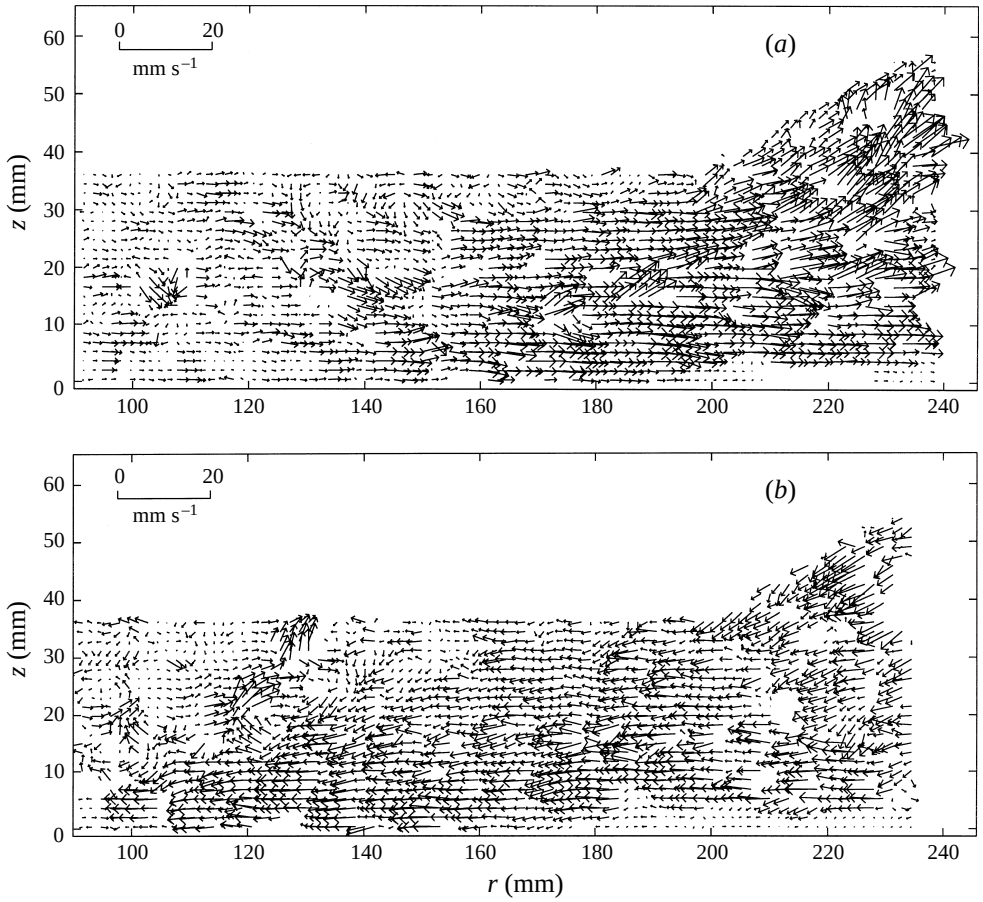

FIGURE 10. Two examples of velocity vector patterns from PIV measurements during exp. 14. (*a*) $t = 666$ s, showing radially outward flow and (*b*) $t = 690$ s, showing radially inward flow.

suppose that for a critical value $f = f_C$, the Rossby radius is so large that only one 'wave' fits around the circumference of the forcing area. Clearly, for experiments for which $f < f_C$, the wavenumber must stay equal to 1. From equation (14), our experiments indicate $5.9R_D = l/n$, with l the length of the shelf break. For the present experiments, $l = 2\pi R$, so that $R_D \approx R/n$, which, for $n = 1$, indicates that when R_D is larger than the length scale R, the horizontal exchange processes can no longer be described by the above scaling arguments. This is indeed the case for the experiments with the two lowest rotation rates in Whitehead (1993). In that situation, one would expect the non-rotating scaling arguments of Sturman & Ivey (1998) to hold. Their equation (26) suggests

$$g'_f = 5\left(\frac{B_0^2}{H}\right)^{1/3}\left(\frac{R}{H}\right)^{2/3} \tag{17}$$

which predicts $g'_f = 8.5 \times 10^{-4}$ m^2 s^{-1} for Whitehead's (1993) low-rotation experiments and compares well with the measured value of the density anomaly in figure 7(*b*) of 11.0×10^{-4} m s^{-2}. Note from table 1 that R_D was always much smaller than R ($= 0.20$ m) so that this non-rotating limit is never achieved in our experiments.

4.3. *Velocity measurements*

From equations (12) and (15), v_{flux}, the characteristic velocity scale within an eddy at steady state, must then be given by

$$v_{flux} \sim (B_0/f)^{1/2}. \tag{18}$$

Note that this is independent of H, which seems plausible since in steady state the eddies at the rim of the convecting region are in good approximation two-dimensional. Velocity measurements have been made during three experiments to check the validity of (18). The measurements are made from the recordings of particle motions illuminated by a vertical light sheet, viewed from the side of the tank, so that only the radial component of the velocity field is measured. The underlying precession motion of the eddy pattern allows us to measure the typical radial velocity of the eddies when they move through the vertical light sheet. Two examples of a flow field obtained from the PIV measurements during one experiment are given in figure 10. Around the shelf break (at $r = 200$ mm), the flow is coherent over the full depth and in figure 10(*a*) radially outward, while in figure 10(*b*) ambient fluid moves into the convecting region. From such vector patterns, the horizontal component of the velocity is averaged over a radial extent of the order of the Rossby radius of deformation (centred around the edge of the heated plate) and over the full depth. Results are given in figure 11(*a–c*) and in table 2 for measurements made when the flow is well into steady state.

The figures show the characteristic radial velocity of the flow induced by a cyclonic eddy as it moves through the thin vertical light sheet. Root-mean-square values are calculated over at least one full period of the signal and compared with equation (18) in table 2. While there is a limited range of f-values, the results clearly show a strong dependence on f and suggest that the functional form of (18) can be quantified as

$$v_{flux} \approx 1.2\,(B_0/f)^{1/2}. \tag{19}$$

It is clear from observations of the convecting region that for these long time scales the exchange between the convecting and ambient fluids is accomplished not by simple advection but rather by an eddy diffusion process. This suggests the following simple model. Suppose that the instability processes on the edge of the convected region affect the complete volume of convecting fluid on a diffusive time scale τ_D, given by

$$\tau_D \sim R^2/K \tag{20}$$

with K a diffusion coefficient, characterized by the product of a typical eddy velocity and length scale. If we represent the velocity scale by the eddy velocity v_{flux} from (19) and the length scale as the radius of the forcing region R (the maximum length scale the eddy field can attain, e.g. Kundu 1990), then

$$K \sim v_{flux}\,R \sim (B_0/f)^{1/2}\,R \tag{21}$$

so that (20) can be written as

$$\tau_D \sim (f/B_0)^{1/2}\,R \tag{22}$$

which is exactly our expression (16) for the steady-state time τ.

The velocity observations show a distinct 'wavelike' behaviour, as a result of the regularity of the array of eddies around the edge of the convected region (see figure 2). The period of this signal can be combined with the wavelength of the eddies to estimate the precession speed of the eddy pattern. In contrast to the characteristic radial velocity induced by the eddies, the precession speed is independent of rotation rate and can be scaled with the estimate of the rim current velocity $(B_0\,R)^{1/3}$ (e.g. Visbeck *et al.* 1996)

$$v_{prec} \approx 0.5\,(B_0\,R)^{1/3}. \tag{23}$$

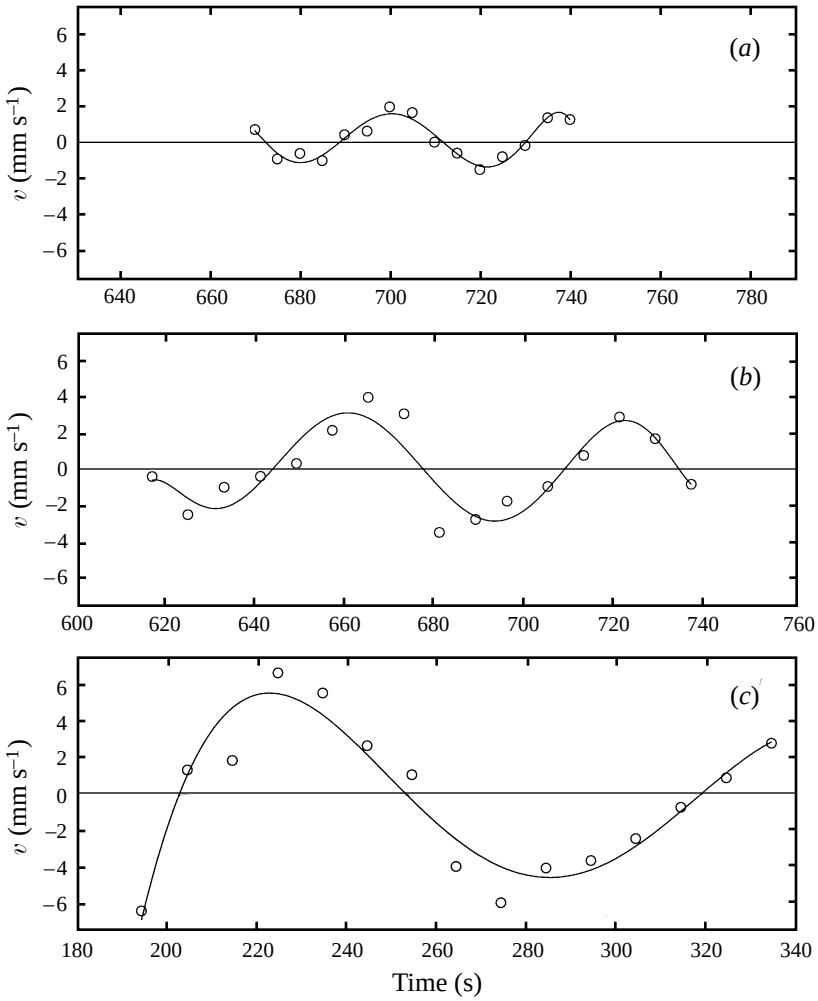

FIGURE 11. Results of radial velocity measurements during steady state for (*a*) exp. 17, $f = 0.900\ \mathrm{s}^{-1}$, $(B_0/f)^{1/2} = 1.02\ \mathrm{mm\ s}^{-1}$; (*b*) exp. 14, $f = 0.402\ \mathrm{s}^{-1}$, $(B_0/f)^{1/2} = 1.98\ \mathrm{mm\ s}^{-1}$; and (*c*) exp. 16, $f = 0.210\ \mathrm{s}^{-1}$, $(B_0/f)^{1/2} = 2.98\ \mathrm{mm\ s}^{-1}$. Solid lines are polynomial fits to the measurements. Measurements started at $t = 2.1\tau$, 3.8τ and 1.8r for (*a*), (*b*) and (*c*), respectively. Flow out of the convecting region is taken positive. The graphs are drawn on the same axes for easy comparison.

Experimental number	f (s^{-1})	$(B_0/f)^{1/2}$ (ms^{-1})	$\overline{(v')^2}^{1/2}$ (ms^{-1})	$\dfrac{\overline{(v')^2}^{1/2}}{(B_0/f)^{1/2}}$	Period (s)	λ (m)	v_{prec} (ms^{-1})	$\dfrac{v_{prec}}{(B_0 R)^{1/3}}$
14	0.402	$1.98\ 10^{-3}$	$2.57\ 10^{-3}$	1.30	60.3	0.209	$3.47\ 10^{-3}$	0.52
16	0.210	$2.98\ 10^{-3}$	$3.82\ 10^{-3}$	1.28	115.0	0.419	$3.64\ 10^{-3}$	0.54
17	0.900	$1.02\ 10^{-3}$	$1.05\ 10^{-3}$	1.03	38.5	0.126	$3.27\ 10^{-3}$	0.48

TABLE 2. Results of velocity measurements (see figure 11)

The present method provides us with information on the typical *radial component* of the velocity field only, which results in data that are independent of the strength of the underlying (azimuthal) precession velocity. This is particularly relevant, since the precession velocity is of the same order of magnitude as (and, with the present choice

of parameter values, mostly larger than) the eddy velocity scale v_{flux}. The above arguments show that there are two velocity scales to be considered: the eddy-induced radial velocity v_{flux}, responsible for the exchange of heat and mass between the convecting region and the ambient, which depends on the rotation rate f; and the precession velocity v_{prec} which scales with the rim current velocity and is therefore independent of f.

5. Discussion and oceanographic applications

The above arguments indicate that the Rossby number, as defined in equation (1), is insufficient to distinguish between the non-rotating and rotation-dominated regimes, because it does not incorporate the horizontal scale of the forcing region R. A better measure is the ratio of the Rossby radius of deformation to the radius of the forcing region R which, using (15), can be expressed as

$$Ro_R = \frac{R_D}{R} = \frac{(g'_f H)^{1/2}}{fR} = \left(\frac{B_0}{f^3 R^2}\right)^{1/4}. \tag{24}$$

Note that this coincides with the square root of the conventional Rossby number (see §1), but now based on the radius of the convected region rather than the fluid depth (see also Maxworthy 1997 and Narimousa 1997). The present results, together with the data from Sugimoto & Whitehead (1983), Whitehead (1993) and Chapman & Gawarkiewicz (1997) are plotted in figure 12 as a function of Ro_R (see also table 1). The density data have been non-dimensionalized with the functional form of (15), so without the numerical constant. This figure indicates that for small values of Ro_R, the non-dimensional steady-state density anomaly can be described by equation (15), with the constant of proportionality ranging between 1.6 ± 0.2 for the present results and 4.5 ± 0.6 for the data of Whitehead (1993). The rather large discrepancy between these extremes warrants further consideration, perhaps by numerical modelling. The average for all data with $Ro_R < 0.5$ is 3.0 ± 1.2. The transition between non-rotating and rotationally controlled convection occurs approximately at a critical value of the above defined Rossby number of $Ro_{R,C} \approx 0.5$. When Ro_R is larger than this critical value, the eddy scale becomes too large with respect to the size of the forcing region R, so that the radial exchange of fluid and heat no longer takes place by the eddy processes.

Typical oceanographic values of the initial parameters in high-latitude coastal seas are $B_0 = 5 \times 10^{-8}\ \mathrm{m^2\ s^{-3}}$ (Schott, Visbeck & Fischer 1993 and Morawitz *et al.* 1996) with $f = 1.4 \times 10^{-4}\ \mathrm{s^{-1}}$ and $R \approx 20$ km. The value of the Rossby number Ro_R is approximately 0.08, well below the critical value above which the influence of the background rotation is unimportant. Even at lower latitudes, for example for the Golfe du Lion region in the North-West Mediterranean, a typical value of Ro_R is around 0.18 (for $B_0 = 1 \times 10^{-7}\ \mathrm{m^2\ s^{-3}}$, $f = 1 \times 10^{-4}\ \mathrm{s^{-1}}$ and $R = 30$ km), still in the rotation-dominated regime.

In general, care should be taken in the comparison of model and field data, since all scaling arguments are based on the assumption that the forcing buoyancy flux is constant, a situation which is seldom achieved in the field. While the present study is confined to homogeneous ambients, Coates *et al.* (1995) demonstrated that the underlying physics of the processes are much the same in the case of background stratification. Applying our results to a shelf region of a polar sea with $R \approx 30$ km, $H \approx 200$ m which is cooled by a surface buoyancy flux of $5 \times 10^{-8}\ \mathrm{m^2\ s^{-3}}$ gives estimates of a steady-state buoyancy anomaly (using equation (15)) of the order of $6 \times 10^{-4}\ \mathrm{m\ s^{-2}}$, corresponding to a temperature difference of approximately 0.65 °C (with

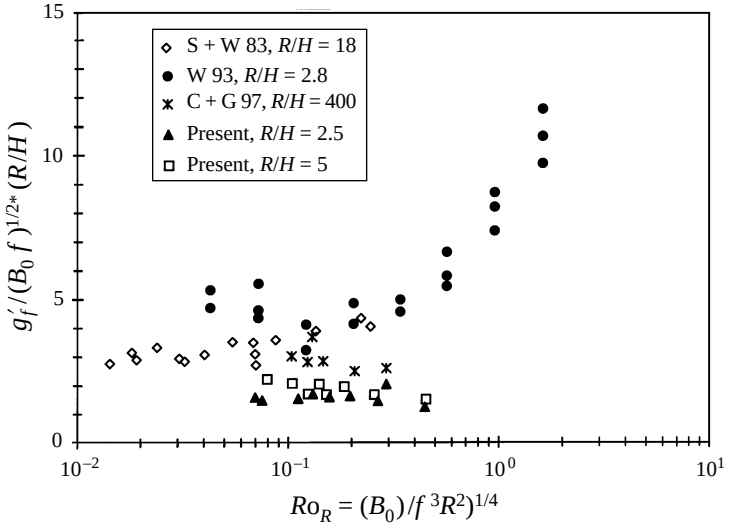

FIGURE 12. Non-dimensional steady-state density anomaly as a function of the Rossby number Ro_R for the present experiments as well as for the results of Sugimoto & Whitehead (1983; S+W 83), Whitehead (1993; W 93) and Chapman & Gawarkiewicz (1997; C+G 97). Transition from rotationally controlled convection to the non-rotating regime occurs at $Ro_R \approx 0.5$.

$\alpha \approx 1 \times 10^{-4}$ °C^{-1}), achieved over a time scale of 57 days (from equation (16)). The horizontal scale of the eddy pattern is then of the order of 15 km. Typical eddy-induced velocities are estimated at 0.023 m s^{-1}, while the translation of the eddy field would occur with a speed of 0.057 m s^{-1}. Morawitz *et al.* (1996) reported on field observations in the Greenland Sea, a region in which the water column is only weakly stratified. They found an average temperature change over the upper 2000 m of the water column on a convective chimney of 0.2 °C, much smaller than our predictions. However, the temperature difference with the fluid surrounding the chimney is of the order of 0.45 °C, so that the total lateral temperature difference is of the same order as in our model. Furthermore, figure 10 of Morawitz *et al.* (1996) shows that the convective processes reached a steady state over a period of 61 days, from January until mid-March. During this period, velocities in the upper 100 m were of the order of 0.07–0.10 m s^{-1}, roughly equal to the algebraic sum of our estimates of the flux and precession velocities. Obviously, the field measurements are unable to discern between these different velocity scales. Unfortunately, the observations of Morawitz *et al.* (1996) could not resolve the dominant eddy scales. Gascard & Clarke (1983) observed eddies in the Labrador Sea under similar forcing conditions with typical length scales of 17 km, almost exactly matching our prediction. These comparisons show that the inclusion of the horizontal dimension R of the convective patch is essential in the estimate of the final density anomaly. Estimates based on simply the rotating scale $(B_0 f)^{1/2}$ or the non-rotating scale $(B_0^2/H)^{1/3}$, which ignore any dependence on R, would result in values that are far too small compared with field data.

The results of the experimental model also allow us to make some predictions on the time scales that can be expected in oceanic convection events. For example, the convective overturning time scale is given by equation (4) which gives for a typical shelf depth $H = 200$ m and $B_0 = 2 \times 10^{-7}$ m^2 s^{-3} a period of 2 h. However, our results show that the onset of lateral exchange occurs on a time scale of several (4–5) overturning times (equation (4) and figure 4*b*), so that, in the field, we can expect to see the influence of baroclinic eddies occurring at around 10 h for the shelf case. Leaman & Schott

(1991) reported on convective overturning events in the top layers of a convective patch (with depths in the order of 10 m) that occur on time scales of 1 h. Equation (4), with the factor 5 and the above value of B_0 gives 1.1 h.

6. Summary and conclusions

Convection in a homogeneous rotating fluid over a model shelf and slope geometry is studied using a laboratory model. Buoyancy forcing is applied, by heating from below, to only the portion of the fluid below the shelf. Initially, the effects of the buoyancy forcing are restricted to the volume of fluid directly above the forcing area. The mean temperature in this volume increases linearly with time until horizontal exchange processes start to affect the convective chimney. In this intermediate regime, part of the heat flux added to the fluid increases the temperature of the fluid above the forcing area, while the remaining portion is transported out of the convecting region by cyclonic eddies, which are formed by the response of ambient fluid to the initial dense outflow over the slope. The cyclonic eddy pattern precesses around the edge of the forced region, following isobaths with the shallower fluid on its right. Eventually the lateral heat exchange becomes so efficient, that all the heat input is transported out of the convective patch, so that a steady state is reached, with no further temperature increase in the convecting region. The most important result of the present experiments with the model shelf and slope is the fact that the final (steady state) value of the density anomaly, the time at which this steady state is reached and the eddy velocity, responsible for the horizontal exchange of heat and mass between the convected region and the ambient, all depend on the strength of the background rotation f, as described by equations (15), (16) and (19), respectively. Furthermore, it is shown that the wavelength of the baroclinic instability pattern depends linearly on the value of the Rossby radius of deformation R_D via equation (14). Finally, the present experiments were all conducted in the rotationally affected (but not controlled) regime, confirming the conclusion of Coates & Ivey (1997) that the transition to rotationally controlled turbulence occurs at Rossby numbers smaller than $Ro^{*1/2} \approx 0.17$.

The cyclonic eddies, whose induced velocity field is primarily responsible for the heat flux between the convecting and ambient regions, stay close to the edge of the convected region due to the presence of the sloping bottom, even at long times after the start of the forcing. This is in sharp contrast to the constant-depth experiments of for example Narimousa (1997), in which the eddies pinch off from the unstable rim current and can subsequently fill the rest of the working fluid. In the present case, the eddy pattern precesses around the edge of the convected region. The precession speed is independent of rotation rate and not simply described by the prediction of Nof (1983), for example, of the speed of isolated eddies on a sloping bottom $C_{Nof} = g'S/f$, with S the bottom slope.

In the present experiments the edge of the forcing region coincided with the position of the shelf break. In the field, the length scales of the wind forcing (50–150 km) and hence buoyancy forcing are often much larger than the width of the continental shelves (20–50 km). Also, submarine canyons or a coastline intersecting the continental shelf can both potentially force considerable mean offshore flow. These various effects should be considered in future (experimental) models. Finally, in the field the buoyancy forcing will almost always be time dependent and/or spatially non-uniform, yielding configurations that should also be considered in future modelling efforts.

We wish to thank Rob Weymouth and Maurice Deusings, who assisted in

performing some of the experiments, and Mike Coates, Tim Finnigan, Prabhath De Silva and Jeff Sturman and three anonymous reviewers for carefully reading the manuscript. Financial support was given by the Australian Research Council. This is Centre for Water Research contribution ED – 1306 PJ.

REFERENCES

Bastin, M. E. & Read, P. L. 1997 A laboratory study of baroclinic waves and turbulence in an internally heated rotating fluid annulus with sloping endwalls. *J. Fluid Mech.* **339**, 173–198.

Brickman, D. 1995 Heat flux partitioning in open-ocean convection. *J. Phys. Oceanogr.* **25**, 2609–2623.

Chapman, D. C. & Gawarkiewicz, G. 1997 Shallow convection and buoyancy equilibration in an idealized coastal polynya. *J. Phys. Oceanogr.* **27**, 555–566.

Clarke, R. A. & Gascard, J. C. 1983 The formation of Labrador Sea Water. Part I: Large-scale processes. *J. Phys. Oceanogr.* **13**, 1764–1778.

Coates, M. J. & Ivey, G. N. 1997 On convective turbulence and the influence of rotation. *Dyn. Atmos. Oceans* **25**, 217–232.

Coates, M. J. & Ivey, G. N. 1998 On continental shelf convection: the influence of an idealised coast. *J. Geophys. Res.* (in Press).

Coates, M. J., Ivey, G. N. & Taylor, J. R. 1995 Unsteady turbulent convection in a rotating stratified fluid: modelling deep ocean convection. *J. Phys. Oceanogr.* **25**, 3032–3050.

Fernando, H. J. S., Chen, R.-R. & Boyer, D. L. 1991 Effects of rotation on convective turbulence. *J. Fluid Mech.* **228**, 513–547.

Gascard, J. C. 1991 Open ocean convection and deep water formation revisited in the Mediterranean, Labrador, Greenland and Weddell Seas. In *Deep Convection and Deep Water Formation in the Oceans* (ed. P. C. Chu & J. C. Gascard), pp. 157–182. Elsevier.

Gascard, J. C. & Clarke, R. A. 1983 The formation of Labrador Sea Water. Part II: Mesoscale and smaller-scale processes. *J. Phys. Oceanogr.* **13**, 1779–1797.

Gawarkiewicz, G. & Chapman, D. C. 1995 A numerical study of dense water formation and transport on a shallow, sloping continental shelf. *J. Geophys. Res.* **100** (C3), 4489–4507.

Hill, A. E. 1996 Spin-down and the dynamics of dense pool gyres in shallow seas. *J. Mar. Res.* **54**, 471–486.

Ivey, G. N., Taylor, J. R. & Coates, M. J. 1995 Convectively driven mixed layer growth in a rotating, stratified fluid. *Deep-Sea Res.* **42**, 331–349.

Jones, H. & Marshall, J. 1993 Convection with rotation in a natural ocean: a study of open-ocean convection. *J. Phys. Oceanogr.* **23**, 1009–1039.

Kundu, P. K. 1990 *Fluid Mechanics*. Academic Press.

Lane-Serff, G. F. & Baines, P. G. 1998 Eddy formation by dense flows on slopes in a rotating fluid. *J. Fluid Mech.* **363**, 229–252.

Leaman, K. D. & Schott, F. A. 1991 Hydrographic structure of the convection regime in the Gulf of Lions: Winter 1987. *J. Phys. Oceanogr.* **21**, 575–598.

Legg, S., Jones, H. & Visbeck, M. 1996 A heton perspective of baroclinic eddy transfer in localized open ocean convection. *J. Phys. Oceanogr.* **26**, 2251–2266.

Legg, S. & Marshall, J. 1993 A heton model of the spreading phase of open-ocean deep convection. *J. Phys. Oceanogr.* **23**, 1040–1056.

Mason, P. J. 1975 Baroclinic waves in a container with sloping end walls. *Phil. Trans. R. Soc. Lond.* A **278**, 397–445.

Maxworthy, T. 1997 Convection into domains with open boundaries. *Ann. Rev. Fluid Mech.* **29**, 327–371.

Maxworthy, T. & Narimousa, S. 1994 Unsteady, turbulent convection into a homogeneous, rotating fluid, with oceanographic applications. *J. Phys. Oceanogr.* **24**, 865–887.

Morawitz, W. M. L., Sutton, P. J., Worcester, P. F., Cornuelle, B. D., Lynch, J. F. & Pawlowicz, R. 1996 Three-dimensional observations of a deep convective chimney in the Greenland Sea during winter 1988/89. *J. Phys. Oceanogr.* **26**, 2316–2343.

Mory, M., Stern, M. E. & Griffiths, R. W. 1987 Coherent baroclinic eddies on a sloping bottom. *J. Fluid Mech.* **183**, 45–62.

Narimousa, S. 1996 Penetrative turbulent convection into a rotating two-layer fluid. *J. Fluid Mech.* **321**, 299–313.

Narimousa, S. 1997 Dynamics of mesoscale vortices generated by turbulent convection at large aspect ratios. *J. Geophys. Res.* **102** (C3), 5615–5624.

Nof, D. 1983 The translation of isolated cold eddies on a sloping bottom. *Deep-Sea Res.* **30**, 171–182.

Raasch, S. & Etling, D. 1997 Unsteady, turbulent convection into a rotating, linearly stratified fluid: Large eddy simulation of deep ocean convection in comparison with laboratory models. Submitted to *J. Phys. Oceanogr.*

Saunders, P. M. 1973 The instability of a baroclinic vortex. *J. Phys. Oceanogr.* **3**, 61–65.

Schott, F. A., Visbeck, M. & Fischer, J. 1993 Observations of vertical currents and convection in the central Greenland Sea during the winter of 1988/89. *J. Geophys. Res.* **98** (C8), 14401–14422.

Schott, F. A., Visbeck, M., Send, U., Fischer, J., Stramma, L. & Desaubies, Y. 1996 Observations of deep convection in the Gulf of Lions, Northern Mediterranean, during the winter of 1991/92. *J. Phys. Oceanogr.* **26**, 505–524.

Send, U. & Marshall, J. 1995 Integral effects of deep convection. *J. Phys. Oceanogr.* **25**, 855–872.

Stevens, C. L. & Coates, M. J. 1994 Applications of a maximised cross-correlation technique for resolving velocity fields in laboratory experiments. *J. Hydraul. Res.* **32**, 195–212.

Sturman, J. J. & Ivey, G. N. 1998 Unsteady convective exchange flows in cavities. *J. Fluid Mech.* **368**, 127–153.

Sugimoto, T. & Whitehead, J. A. 1983 Laboratory models of bay-type continental shelves in the winter. *J. Phys. Oceanogr.* **13**, 1819–1828.

Visbeck, M., Marshall, J. & Jones, H. 1996 Dynamics of isolated convective regions in the ocean. *J. Phys. Oceanogr.* **26**, 1721–1734.

Whitehead, J. A. 1993 A laboratory model of cooling over the continental shelf. *J. Phys. Oceanogr.* **23**, 2412–2427.

Whitehead, J. A., Marshall, J. & Hufford, G. E. 1996 Localized convection in rotating stratified fluid. *J. Geophys. Res.* **101** (C11), 25705–25721.

Whitehead, J. A., Stern, M. E., Flierl, G. R. & Klinger, B. A. 1990 Experimental observations of baroclinic eddies on a sloping bottom. *J. Geophys. Res.* **95** (C6), 9585–9610.